Analysis of Thomson scattered light from an arc plasma jet

G. Gregori, U. Kortshagen, J. Heberlein, and E. Pfender
Department of Mechanical Engineering, University of Minnesota, Minneapolis, Minnesota 55455
(Received 9 August 2001; published 2 April 2002)

In this paper we present an analysis of Thomson scattered light from an arc plasma jet. Our approach goes beyond the standard random-phase approximation (RPA) and provides more consistent data for the electron temperature and density in plasmas that are weakly nonideal and collisional. The theory is based on a memory function formalism for the spectral density function with the use of the three lowest-order frequency-moment sum rules. These moments are then corrected for temperature inhomogeneities in the scattering volume. The proposed interpretation of scattering data is compared with the RPA result and with the standard Bhatnagar-Gross-Krook collisional model for the dynamic structure factor. It is shown that the obtained electron temperature values are closer but not equal to local thermodynamic equilibrium temperature values extracted from spectroscopic measurements.

DOI: 10.1103/PhysRevE.65.046411 PACS number(s): 52.70.Kz, 42.62.Fi, 61.20.Ne, 52.75.Hn

I. INTRODUCTION

The dynamic structure factor, or spectral density function, is a fundamental quantity that describes the correlations among particles in a plasma, as the individual and/or collective behavior of electrons and ions remains imprinted in it. Thermodynamic and transport properties can then be derived from the spectrum of the density fluctuations [1]. Of particular interest is the electron density-density correlation, since it can be directly probed in a plasma using Thomson laser scattering (see, e.g., Pavlov [2]) allowing the simultaneous measurement of electron density and temperature if an accurate model for the dynamic structure factor is available. In the early work of Salpeter [3], the spectrum of the electron-density fluctuations was obtained for an ideal, uniform and collisionless plasma [4–6]. We will refer to this model as the random-phase approximation (RPA). The RPA has then been successfully applied for measurements of electron temperature and density using Thomson scattering in several plasma environments [4,6] with the exception of thermal arcs and atmospheric plasma jets [7–9]. Comparison between the RPA model and the experimentally determined dynamic structure factors in thermal arcs and atmospheric plasma jets provides electron temperature values that are inconsistent with the local thermodynamic equilibrium (LTE) temperature values extracted from other well-established diagnostics, such as emission spectroscopy or enthalpy probes [7]. In addition, some authors [9,10] have recently reported experiments showing dependence of the derived electron temperature values on the scattering angle. In those experiments, density fluctuations were probed at a wavelength for which a straightforward interpretation of light-scattering data based on the random-phase approximation may not always be accurate. Indeed, similar experiments conducted at different wavelength showed no dependence on the scattering angle [10]. Inclusion of electron-ion collisions [9,10] or correction for inhomogeneities in the scattering volume [9] have been proposed as possible mechanisms responsible for the observed angular dependence in the analysis of measured data using the RPA. However, such approaches are still heuristic without rigorous theoretical justifications.

The degree of coupling is usually described by the ratio of the potential to the kinetic energy per particle (see, e.g., Ichimaru [11]) and in singly ionized systems is written as $\Gamma = e^2/4\pi\epsilon_0 k_B T d$, where T is the electron temperature and $d = (3/4\pi n)^{1/3}$ is the ion-sphere radius, with $n = n_e \simeq n_i$ the electron (or ion) density. The Debye length in a two-component plasma is given in terms of the coupling parameter as $\lambda_D = (\epsilon_0 k_B T/2e^2 n)^{1/2} = (d^2/6\Gamma)^{1/2}$. The factor $\sqrt{2}$ that appears in the definition of the Debye length accounts for both electron and ion screening. The number of electrons inside a sphere of radius λ_D is $\Lambda = 4\pi n \lambda_D^3/3$. In an ideal plasma $\Lambda \gg 1$ (or $\Gamma \ll 1$) and the Coulomb screening is well represented by the Debye length. In the opposite case, $\Lambda \ll 1$ (or $\Gamma \gg 1$), the potential energy dominates over the kinetic energy and λ_D does not relate anymore with the screening of the electrostatic forces. These plasmas are then called strongly coupled. For typical conditions in atmospheric plasma jets, $\Gamma \sim 0.05$–0.1, corresponding only to about $\Lambda \sim 2$–4 electrons in the Debye sphere. It is then clear that, at these couplings, nonideal corrections to the RPA may become important since the number of electrons within the Debye sphere remains quite small. Typically, we should expect the RPA to be valid for $\Lambda \gtrsim 10$. Moreover, as the degree of coupling increases, the collision rate between charged particles becomes progressively more important. However, calculating the correct value for the collision frequency in a weakly nonideal plasma requires some attention. In this respect, we should notice that in an ideal plasma the electron-ion collision frequency is mainly determined by long-range Coulomb forces. On the other hand, as Γ approaches unity, short-range interactions become significant. An estimate of ν_{ei}, the electron-ion collision frequency, in this transition region has been recently discussed by Valuev *et al.* [12]. We see that for typical values of the coupling parameter which are found in plasma jets, $\nu_{ei}/\omega_p \simeq 0.01$–$0.02$, where $\omega_p = (e^2 n/\epsilon_0 m)^{1/2}$ is the electron plasma frequency. We are then in a region where the use of a collisionless model for the dynamic structure factor may be questionable.

II. THEORY

A. Charge-charge correlation function

In a Thomson scattering experiment, the intensity of the scattered light is proportional to $S_{ee}(k,\omega)$, the electron density-density correlation function, which represents the spectrum of the longitudinal density fluctuations. In the low-energy (nonrelativistic) limit, $k=|\mathbf{k}|=|\mathbf{k}_i-\mathbf{k}_s| =(4\pi/\lambda_i)\sin(\theta/2)$, where $\mathbf{k}_i$ and $\mathbf{k}_s$ are the incident and scattered wave number, respectively, λ_i is the incident laser wavelength, and θ the scattering angle. The difference between the scattered and the incident photon frequency is $\omega =\omega_s-\omega_i$. In order to describe the collective modes of electrons and ions, we introduce the time-dependent density of species α,

$$\rho_\alpha(\mathbf{r},t)=\sum_{s=1}^{N}\delta(\mathbf{r}-\mathbf{r}_s^{(\alpha)}(t)), \tag{1}$$

where $\alpha=i$ (ions) or $\alpha=e$ (electrons). The total number of particles of type α in the system is N, and the time-dependent position vector of the sth particle of species α is $\mathbf{r}_s^{(\alpha)}(t)$. The Fourier components of the density are thus

$$\rho_\alpha(\mathbf{k},t)=\sum_{s=1}^{N}\exp[i\mathbf{k}\cdot\mathbf{r}_s^{(\alpha)}(t)]. \tag{2}$$

The electron-electron density correlation is defined as

$$S_{ee}(k,\omega)=\frac{1}{2\pi N}\int_{-\infty}^{\infty}e^{i\omega t}\langle\rho_e(\mathbf{k},t)\rho_e(-\mathbf{k},0)\rangle dt, \tag{3}$$

where $\langle\ldots\rangle$ denotes a thermal average. Having implicitly assumed isotropy, the dynamic structure depends only on the magnitude of k and not on its direction.

The correlation function $S_{ee}(k,\omega)$ has two main contributions [5,2]: a low-frequency part related to the light scattered from electrons that closely participate in the screening of the ions, and a high-frequency ($\omega\gtrsim kv_t$, with v_t the electron speed) term arising from free electrons that do not participate in the ion screening. In our experiments we probed the high-frequency part of $S_{ee}(k,\omega)$, representing electrons oscillating in the vicinity of the plasma frequency, while the low-frequency satellite remained spectrally unresolved. Using the fluctuation-dissipation theorem, $S_{ee}(k,\omega)$ is expressed in terms of the plasma dielectric response function $\epsilon(k,\omega)$, and in the high-frequency limit we have [5]

$$S_{ee}(k,\omega)\simeq-\frac{1}{\pi\omega}\frac{2k^2}{k_D^2}\mathrm{Im}\left[\frac{1}{\epsilon(k,\omega)}\right], \tag{4}$$

where k_D is the inverse of the Debye length. The right-hand side of Eq. (4) is related to the linear response of the plasma to an external electric field. This is clarified by introducing the charge-charge correlation function

$$S_{ZZ}(k,\omega)=\frac{1}{4\pi N}\int_{-\infty}^{\infty}e^{i\omega t}\langle\rho(\mathbf{k},t)\rho(-\mathbf{k},0)\rangle dt, \tag{5}$$

with $\rho(\mathbf{k},t)=\rho_i(\mathbf{k},t)-\rho_e(\mathbf{k},t)$ the charge-density distribution. The charge-charge correlation function naturally gives the spectrum of the charge fluctuations, and they are related to the plasma dielectric function by the fluctuation-dissipation theorem [13]

$$S_{ZZ}(k,\omega)=-\frac{1}{\pi\omega}\frac{k^2}{k_D^2}\mathrm{Im}\left[\frac{1}{\epsilon(k,\omega)}\right]. \tag{6}$$

Thus, in the high-frequency regime, we clearly have $S_{ee}(k,\omega)=2S_{ZZ}(k,\omega)$.

Since our measurement apparatus detects only the high-frequency feature of the spectrum, the measured scattered light intensity is then proportional to only $S_{ZZ}(k,\omega)$.

B. Frequency moments

The advantage of the proposed approach is that frequency moment sum rules of the charge structure factor are easily obtained. $S_{ZZ}(k,\omega)$ is even in frequency, thus its odd frequency moments are all zero. Defining the even frequency moments as

$$\Omega_{2n}=\int\omega^{2n}S_{ZZ}(k,\omega)d\omega, \tag{7}$$

then we have for the first three moments [2,13–15]

$$\Omega_0=S_{ZZ}(k), \tag{8}$$

$$\Omega_2=\frac{1}{2}\left(\frac{k_BT}{m}k^2+\frac{k_BT}{M}k^2\right), \tag{9}$$

$$\begin{aligned}\Omega_4=\frac{1}{2}\Bigg[&\frac{3k_B^2T^2}{m^2}k^4+\frac{nk_BTk^2}{3m^2}\int\nabla^2v_{ee}(r)g_{ee}(r)d\mathbf{r}\\&+\frac{nk_BTk^2}{3m^2}\int\nabla^2v_{ei}(r)g_{ei}(r)d\mathbf{r}\\&-\frac{nk_BTk^2}{m^2}\int\exp(i\mathbf{k}\cdot\mathbf{r})g_{ee}(r)(\hat{\mathbf{k}}\cdot\boldsymbol{\nabla})^2v_{ee}(r)d\mathbf{r}\\&+\frac{3k_B^2T^2}{M^2}k^4+\frac{nk_BTk^2}{3M^2}\int\nabla^2v_{ii}(r)g_{ii}(r)d\mathbf{r}\\&+\frac{nk_BTk^2}{3M^2}\int\nabla^2v_{ei}(r)g_{ei}(r)d\mathbf{r}\\&-\frac{nk_BTk^2}{M^2}\int\exp(i\mathbf{k}\cdot\mathbf{r})g_{ii}(r)(\hat{\mathbf{k}}\cdot\boldsymbol{\nabla})^2v_{ii}(r)d\mathbf{r}\\&+\frac{2nk_BTk^2}{mM}\int\exp(i\mathbf{k}\cdot\mathbf{r})g_{ei}(r)(\hat{\mathbf{k}}\cdot\boldsymbol{\nabla})^2v_{ei}(r)d\mathbf{r}\Bigg],\end{aligned} \tag{10}$$

where $\hat{\mathbf{k}}$ is a unit vector parallel to $\mathbf{k}$, M is the ion mass, $v_{\alpha\beta}(r)$ is the interaction potential between a particle of species α and a particle of species β separated by a distance r. The pair distribution functions are given by $g_{\alpha\beta}(r)$. These moments have also a clear physical interpretation [1]: the zeroth moment gives the total power in the fluctuations at a given scattering angle, the second moment is a restatement of the conservation of the number of particles and the fourth moment includes the effects of pair interactions. We shall notice that the frequency moments reported here are strictly valid only if the electron and the ion temperatures are equal, i.e., $T_e=T_i=T$. Generalization to a two-temperature plasma is straightforward. However, since our interest focuses only on the fast-moving electrons, then in the limit $m \ll M$, the relevant temperature in describing frequency moments is just given by $T=T_e$.

The static structure, $S_{ZZ}(k)$, does not have a simple representation, and, in general, can be obtained only from molecular dynamics simulations [16] or the hypernetted chain equation [17,20]. However, since a weakly nonideal plasma does not have a short-range order, characteristic of highly correlated systems ($\Gamma \gg 1$), it is reasonable to assume a simple linear Debye-Hückel form for the pair distribution functions [18,19], along with the bare Coulomb potential describing the charged particles interaction. The use of a bare Coulomb potential is, in fact, unreasonable if we want to preserve the two-component plasma system from collapsing (see, e.g., Baus and Hansen [20]) as particles of opposite charge may stay arbitrarily close together. In reality, quantum diffraction (i.e., the Pauli exclusion principle) prevents this collapse from happening by reducing the effective potential at a separation distance of the order of the de Broglie thermal wavelength [13,21]. Since the electron thermal wavelength remains much shorter than the ion-sphere radius at typical densities of our plasma, we can regard quantum diffraction effects as higher-order corrections in the Coulomb potential. Under these conditions, and since $m \ll M$, the previous expressions for the frequency moments considerably simplify (see also Refs. [22,23])

$$\Omega_0 \simeq \frac{k^2}{k^2+k_D^2}, \tag{11}$$

$$\Omega_2 \simeq \frac{1}{2}(kv_t)^2, \tag{12}$$

$$\Omega_4 \simeq \frac{1}{2}[3(kv_t)^4+(kv_t)^2\omega_p^2], \tag{13}$$

where $k_D=(2e^2n/\epsilon_0 k_B T)^{1/2}$ is the inverse of the Debye length and $v_t=(k_B T/m)^{1/2}$ is the electron speed.

Following the approach described by Hansen *et al.* [24], we can rewrite the response function in terms of an unknown *memory function* $N(k,\omega)=N'(k,\omega)+iN''(k,\omega)$. The charge structure factor can then be expressed in a very general form as

$$S_{ZZ}(k,\omega)=\frac{1}{2\pi}\frac{(kv_t)^2N'(k,\omega)}{[\omega^2-\omega_0^2-\omega N''(k,\omega)]^2+[\omega N'(k,\omega)]^2}, \tag{14}$$

where $\omega_0^2=\Omega_2/\Omega_0$. Here, $N'(k,\omega)$ represents the damping of the electron plasma wave and $N''(k,\omega)$ its dispersion. In a phenomenological approach, the memory functions are chosen such that the correct three lowest-order frequency-moment sum rules are exactly reproduced by the charge-charge correlation function. The advantage of such a representation is that we do not need anymore an exact microscopic theory to derive the spectrum of the longitudinal density fluctuations. Conversely, the spectrum is obtained in a form that is phenomenologically self consistent. Assuming that the memory functions are much simpler objects than the density correlation itself, we adopt the following Gaussian form for the damping function [24]:

$$N'(k,\omega)=\sqrt{\pi}\tau_k(\omega_{1l}^2-\omega_0^2)\exp(-\tau_k^2\omega^2), \tag{15}$$

where $\omega_{1l}^2=\Omega_4/\Omega_2$ and τ_k is the (k-dependent) relaxation time for the damping of the collective modes. From the analytic properties of the response function, and hence of $N(k,\omega)$, the dispersion memory function $N''(k,\omega)$ is then obtained from $N'(k,\omega)$ with the help of the Kramers-Kronig relation [24,1]

$$\begin{aligned} N''(k,\omega) &= -\mathrm{P}\frac{1}{\pi}\int\frac{N'(k,\omega')}{\omega'-\omega}d\omega' \\ &= 2\tau_k(\omega_{1l}^2-\omega_0^2)\exp(-\tau_k^2\omega^2)\int_0^{\tau_k\omega}\exp(y^2)dy, \end{aligned} \tag{16}$$

with P denoting the principal part of the integral. The relaxation time τ_k is related to the sixth moment of the charge-charge correlation function [22]. We have

$$\omega_{2l}^4=\frac{\Omega_6}{\Omega_2}=\omega_{1l}^4+\frac{\omega_{1l}^2-\omega_0^2}{2\tau_k^2}. \tag{17}$$

However, explicit expressions for Ω_6 in terms of the electron temperature and the electron density are difficult to obtain since they involve triplet correlation functions in slowly convergent integrals [15]. In our analysis then, the relaxation time is left as an additional parameter in the expression for the correlation function. In Fig. 1 theoretical line shapes for $S_{ee}(k,\omega)$ in the high-frequency limit have been calculated from the memory function formalism (MFF) model for different values of τ_k. The theoretical spectral density in the RPA approximation is also plotted for comparison. We clearly see significant differences between the MFF and RPA models. Since, in our formulation, the relaxation time is an adjustable parameter, it can be phenomenologically varied in order to change the damping mechanism of the collective modes. In absence of a reliable microscopic theory, the ad-

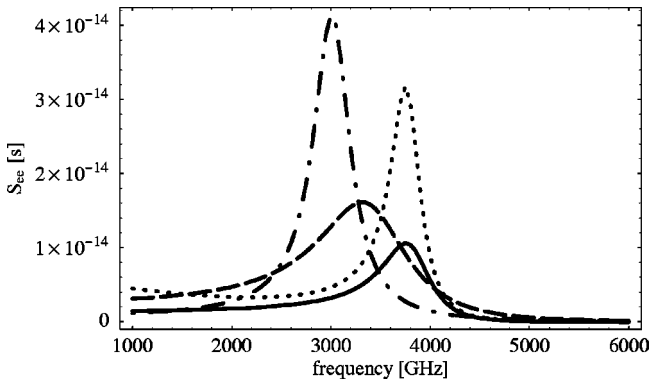

FIG. 1. Theoretical spectral density function $S_{ee}(k,\omega)$ at $\theta=90°$ for $T=15\,000$ K and $n=1.0\times10^{23}$ m^{-3}: RPA (solid line); MFF with $\tau_k=1.0\times10^{-14}$ s (dash-dotted line); MFF with $\tau_k=3.0\times10^{-14}$ s (dashed line); MFF with $\tau_k=6.0\times10^{-14}$ s (dotted line).

vantage of a phenomenological approach is that the details of these physical processes are all lumped together in one single parameter.

C. Inhomogeneous systems

From the previous analysis we have derived the complete set of equations required to describe charge, or high-frequency density fluctuations in a homogeneous system, i.e., assuming that in the volume under consideration, large-scale variations of the plasma properties, specifically electron temperature and density, remain negligible. The charge structure factor is thus determined by ω_0^2, ω_{1l}^2 and the relaxation time τ_k. The intensity of the scattered light, as measured by the detection apparatus, is given by

$$I(k,\omega)=A\int h_i(\omega')S_{ZZ}(k,\omega'-\omega)d\omega'+B, \qquad (18)$$

where h_i is the instrument function. Following van de Sanden *et al.* [25], we estimate the instrument function using the measured light signal from an argon jet at room temperature. We find that h_i is well represented by a Lorentzian with 30 GHz half width. A and B are parameters that also include the response of the experimental apparatus, the total number of scattering particles (i.e., the electron density) and their temperature. At a given scattering angle (or wave number) the full set of unknowns ω_0^2, ω_{1l}^2, τ_k, A, and B is determined by calculating the convolution of $S_{ZZ}(k,\omega)$ with the instrument function using fast Fourier transform and then performing a Levenberg-Marquardt nonlinear fitting [26] of $I(k,\omega)$ with the experimental line shape. The fitting result for the parameters $\omega_0^2,\omega_{1l}^2,\tau_k$ is actually independent from A and B which only represent a scale term of the instrument response and the baseline correction. As mentioned, if the system is uniform, electron temperature and electron density can be obtained from ω_0^2 and ω_{1l}^2 using Eqs. (11)–(13).

The situation is, obviously, more complex if the system exhibits nonuniformities, as the expressions for the frequency moments need to be corrected in order to include additional broadening of the line shape. Effects of inhomogeneity in the scattering volume on the Thomson signal have been previously reported by Gregori *et al.* [9] and by Rozmus *et al.* [27] (and references therein). Typically, thermal plasma jets exhibit strong density and temperature gradients and with the large laser beam waist diameter used in our experiment in order to reduce inverse bremsstrahlung heating, large-scale variations of the plasma properties in the scattering volume may, to some extent, modify the measured line shapes [9]. Since the measured signal is proportional to the electron density times the spectral density function, the high-density region in the scattering volume will largely contribute to the measured signal. Thus, it is expected that the electron density obtained from Thomson scattering be representative of the peak densities in the probed region. On the other hand, in the presence of temperature inhomogeneities, the measured dynamic structure will be given by

$$S_{ZZ}(k,\omega)=\int \Theta_k(T')S_{ZZ}(k,\omega;T')dT', \qquad (19)$$

where we have explicitly indicated the *local* temperature dependence in $S_{ZZ}(k,\omega;T')$. The contribution of regions at different temperature in the scattering volume is represented by the temperature distribution function Θ_k. In a homogeneous system, $\Theta_k(T')=\delta(T-T')$. In a very simple picture, we can regard the homogeneous system as the limiting case of a normalized steplike temperature distribution

$$\Theta_k(T')=\frac{1}{T\chi_k}, \qquad (20)$$

if $T(1-\chi_k)<T'<T$, and $\Theta_k(T')=0$ otherwise. Here, χ_k is an angle-dependent parameter which indicates the extent of temperature variations. In the limit $\chi_k\to0$, the homogeneous case is indeed reproduced. The average temperature in the scattering volume is given by

$$T_{av}=\int T'\Theta_k(T')dT'=T(1-\chi_k/2). \qquad (21)$$

This shows that the average temperature is a function of the scattering angle, since at large angles (back scattering) and small angles (forward scattering) we expect to probe a larger volume than at 90° scattering angle. From the given temperature distribution, it is easy to calculate the corrected frequency moments of the charge-charge correlation function under the same approximations that led to Eqs. (11)–(13). We then obtain for the *normalized* moments

$$\omega_0^2=-\frac{\omega_p^2\chi_k(1-\chi_k/2)}{\ln\left(1-\dfrac{k_D^2}{k^2+k_D^2}\chi_k\right)}, \qquad (22)$$

$$\omega_{1l}^2=3(kv_t)^2\frac{1-\chi_k+\chi_k^2/3}{1-\chi_k/2}+\omega_p^2. \qquad (23)$$

This completes the full set of equations necessary to derive electron temperature and density from the experimental data.

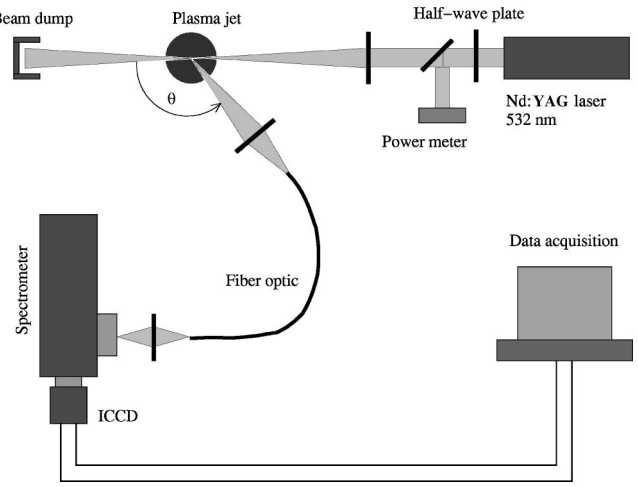

FIG. 2. Schematic of the experimental setup.

III. EXPERIMENT

We have measured spectral density functions in atmospheric plasma jets in order to compare theoretical models with Thomson laser scattering results. The experimental setup is shown in Fig. 2. A dc torch operating at atmospheric pressure with a pure argon flow rate of 35.0 l/min, or a mixture of argon at 30.0 l/min and helium at 28.4 l/min has been used to generate the jet, which is probed in the center 3 mm downstream from the nozzle exit with a *Q*-switched frequency-doubled (532 nm) Nd:Yag laser. The pulse duration is 10 ns with a repetition rate of 20 Hz. The torch has been operated with an arc current of 600 A at 30 V (with pure argon) or 40 V (with an argon-helium mixture). The jet diameter at the nozzle exit is approximately 8 mm. Data collection is performed at various scattering angles with a visible-light fiber bundle and then imaged onto the 100 μm entrance slit of a monochromator equipped with a 140×120 mm^2, 1800 groove/mm holographic grating. The line profile is then measured with a two-dimensional intensified charge-coupled device gated array detector. The plasma jet is aligned perpendicularly to the scattering plane, and to maximize the signal, the direction of polarization of the incident light has been rotated along the direction of the jet axis with a half-wave plate. Additional details of the experimental setup can be found in Gregori *et al.* [9].

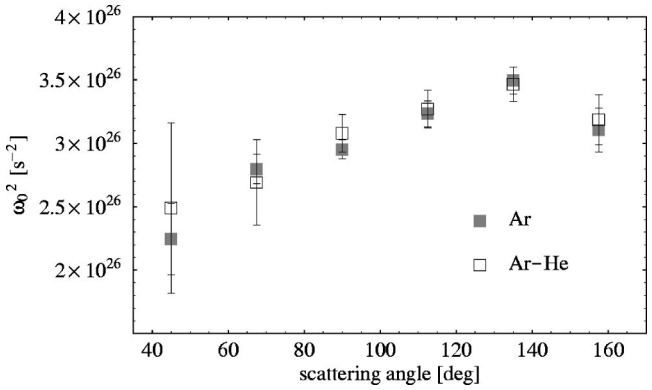

FIG. 3. Normalized moment ω_0^2 as a function of the scattering angle (in degrees) for the pure argon jet and the argon-helium mixture.

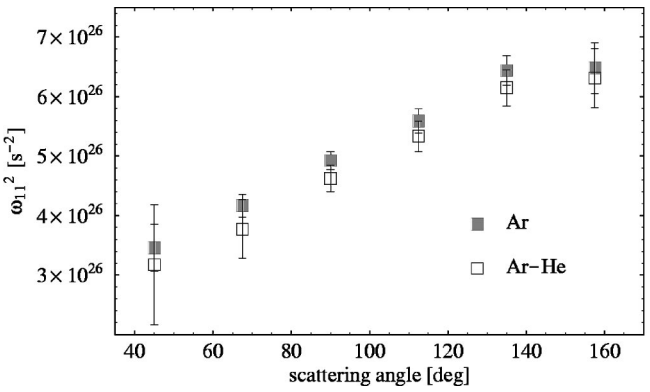

FIG. 4. Normalized moment ω_{1l}^2 as a function of the scattering angle (in degrees) for the pure argon jet and the argon-helium mixture.

The characteristic time scale for electron heating in a laser pump field is given by $\tau_H \sim (v_t/v_E)^2/\nu_{ei}$ [28,29], where $v_t = (k_B T/m)^{1/2}$ is the electron thermal speed and v_E is the velocity with which the electrons oscillate in the laser pump field. For typical laser energies (0.05–0.4 J/pulse) and waist diameter ($\gtrsim$2 mm) used in our experiment, τ_H is considerably longer than the laser-pulse duration, leading to a negligible inverse bremsstrahlung heating of the electrons (see, e.g., Snyder *et al.* [10]).

IV. RESULTS

In this section we present electron temperatures and densities from the experimental data following the suggested theoretical approach based on the memory function formalism. Equation (18) is used to fit the experimental data in order to extract the *normalized* moments ω_0^2 and ω_{1l}^2. The results are plotted in Figs. 3 and 4. Since ω_{1l}^2, in the weak coupling limit, is independent on the specific form for the pair correlation function, it can be easily fitted for T and n using Eq. (23) where $\chi_k(T,n)$ is given by Eq. (22). Values between consecutive scattering angles are interpolated with polynomials of order 3. Best-fit curves obtained from this model are plotted in Figs. 5 and 6. As we can see, the MFF

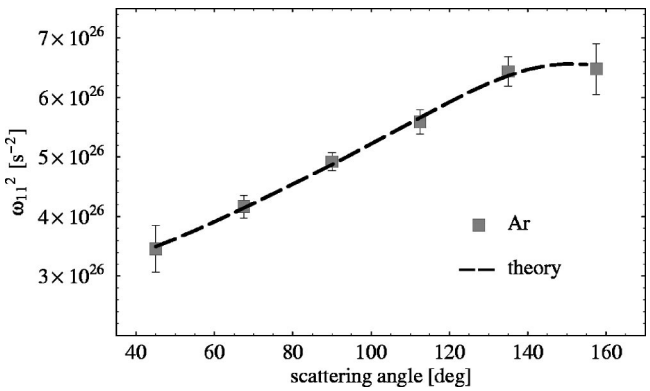

FIG. 5. Best-fit curve of ω_{1l}^2 given by Eq. (23) vs scattering angle (in degrees). The plasma gas is argon at 35 l/min.

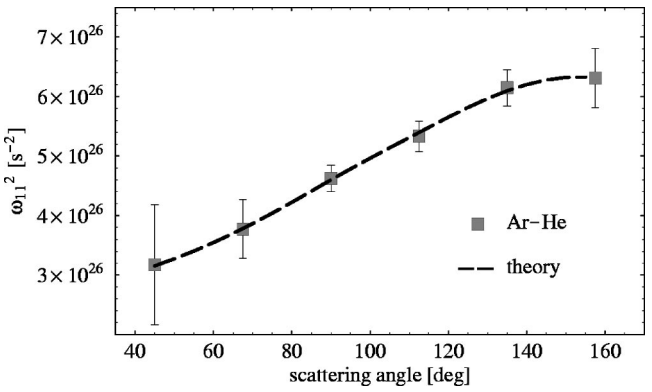

FIG. 6. Best-fit curve of ω_{1l}^2 given by Eq. (23) vs scattering angle (in degrees). The plasma gas is argon at 30 l/min and helium at 28.4 l/min.

model corrected for temperature nonuniformities shows excellent agreement with the data. From the best fit, an electron density $n=9.3\times10^{22}$ m^{-3} is obtained for a pure argon jet, and a density $n=8.2\times10^{22}$ m^{-3} is obtained for the argon-helium mixture. Average electron temperature values, calculated from Eq. (21) are then plotted in Fig. 7. We see that at small and large scattering angles the average temperature in the collection volume slightly decreases as a result of larger volumes being probed. The maximum temperature in the scattering volume is shown in Fig. 8. It can be seen that, within the experimental confidence intervals, the maximum temperature values are almost independent on the scattering angle. The method proposed in this paper hence resolves the problem of angle-dependent results of the Thomson scattering temperature measurements that were clearly unphysical. This result thus lends further credibility to the method presented here.

V. DISCUSSION

We compare the temperature and density values obtained with three different models for the spectral density function: the standard RPA, the Bhatnagar-Gross-Krook (BGK) approximation [6], and the memory function formalism (MFF) described above. The main difference between the RPA and

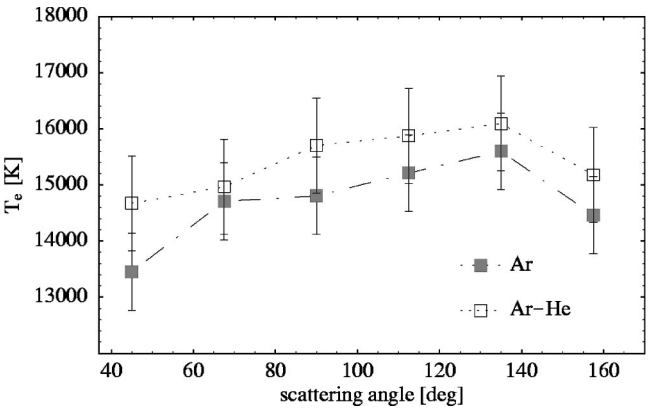

FIG. 7. Average electron temperature, from Eq. (21), in the scattering volume.

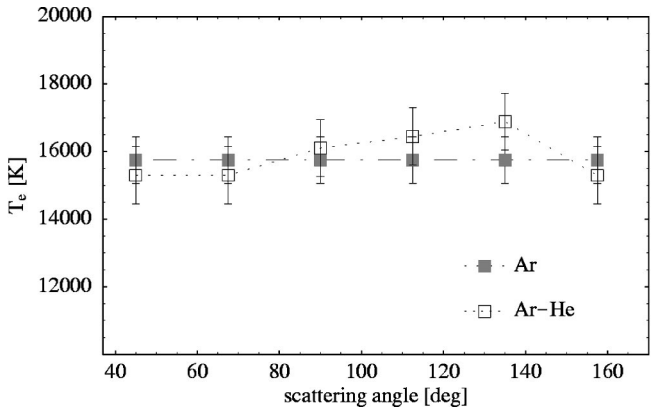

FIG. 8. Maximun electron temperature in the scattering volume.

the BGK approximation is that the former does not consider collisions, thus the density fluctuations are simply obtained by the solution of the Vlasov equation. Instead, in the BGK model, an approximate form is introduced for the collision integral in the Boltzmann equation. However, the BGK collision operator is designed primarily to describe the effects of weak electron-neutral collisions on the spectral density function, and its extension in the strong electron-ion collision regime may be inaccurate. In addition, both the RPA and the BGK models calculate the spectral density function using the principle of superposition of dressed particles [5] which requires that the condition $\Gamma\ll1$ (ideal plasma) must be satisfied.

We shall observe that at $k\ll k_D$ (small scattering angles, or large laser wavelength) we probe the density fluctuations far in the collective regime. As noticed by Snyder *et al.* [10], here collisional damping is probably dominant, and the use of either RPA or BGK models is questionable. Conversely, in the region $k\sim k_D$ (large scattering angles, or small laser wavelength) there occurs the transition from a kinetic to a fluid behavior of the plasma particles [20]. This is the regime where nonideal effects are most important [30], and again both RPA and BGK models may become invalid. Instead, the phenomenological memory function approach that we have described in this paper does not rely on a particular microscopic theory for the derivation of the spectral density function, and it is valid at all scattering angles.

The experimental line shape obtained at $\theta=90°$ for the argon (30 l/min) helium (28.4 l/min) plasma jet is plotted in Fig. 9, along with the best-fit results obtained from the three models that we have discussed. We see, in all cases, very good fits to the experimental signal, with negligible differences among them in the fitted lineshape. However, quite different values for the electron temperature are derived from these models. This is shown in Figs. 10 and 11. Differences in the electron density are instead less pronounced. Typically, for the pure argon jet, we get $n=9.4\times10^{22}$ m^{-3} (MFF), $n=6.2\times10^{22}$ m^{-3} (RPA), $n=6.4\times10^{22}$ m^{-3} (BGK), while for the argon-helium mixture $n=8.2\times10^{22}$ m^{-3} (MFF), $n=6.8\times10^{22}$ m^{-3} (RPA), $n=7.1\times10^{22}$ m^{-3} (BGK). We clearly see that both the RPA and BGK models show a strong dependence of the temperature values on the scattering angle. This behavior is much less pronounced in the memory

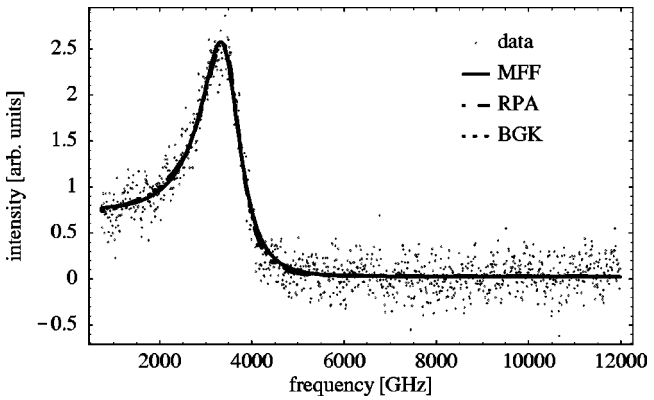

FIG. 9. Experimental line shape obtained at $\theta=90°$ for the argon-helium jet mixture by accumulating several laser pulses during 1 min exposure time. Background subtraction, flat field correction, and removal of the central Rayleigh scattered signal has been performed.

function formalism corrected for temperature inhomogeneities, with a decrease in the average temperature at small and large scattering angles. Small scattering angles correspond to the region $k_D/k\sim 4-6$, where collisional broadening is important. At larger scattering angles ($k_D/k\sim 2$) the differences among the models are less pronounced, however, especially for the pure argon jet, MFF temperatures remain substantially different from the RPA and the BGK ones. As discussed, in this region we start seeing nonideal coupling effects. Excitation temperatures close to 12 000–14 000 K have been obtained from emission spectroscopy measurements [31] in similar plasmas at the same axial position. Differences between emission spectroscopy and Thomson scattering results based on the MFF approach still exist, suggesting the possibility of deviations from LTE in arc plasma jets. However, the extent of such deviations is smaller than the value reported by Snyder *et al.* [10] using the RPA in the data analysis at large scattering angles, an indication that a correct model for the spectrum of the density fluctuation is crucial for interpreting the physical properties of weakly coupled arc plasma jets.

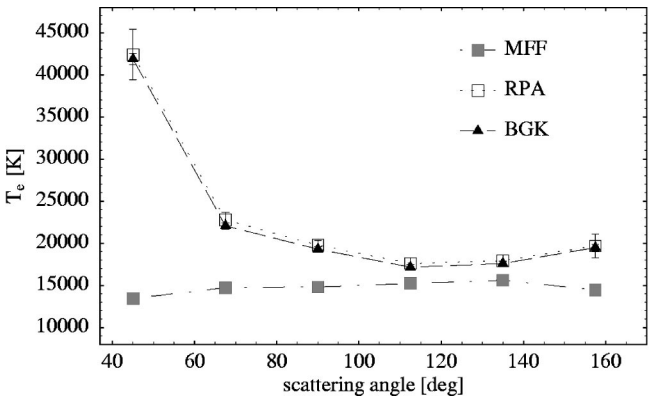

FIG. 10. Electron temperature derived from the models described in the text vs scattering angle (in degrees). In the MFF average temperatures are plotted. The plasma gas is argon at 35 l/min.

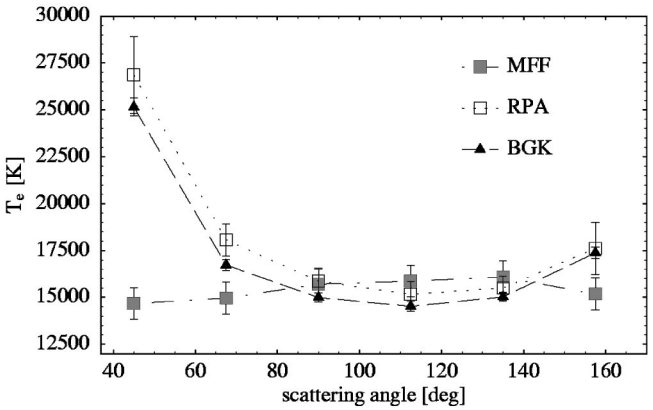

FIG. 11. Electron temperature derived from the models described in the text vs scattering angle (in degrees). In the MFF average temperatures are plotted. The plasma gas is argon at 30 l/min and helium at 28.4 l/min.

From previous studies on the effect of coupling $\Gamma\sim 0.05-0.1$ on the structure of the spectral density function [32] it was shown that the experimental electron features are broader than expected from the RPA. It was concluded that the broadening was due to density inhomogeneities and, to some extent, collisions. However, no direct justification was offered and nonideal effects may also have had some influence. Even if large density inhomogeneities in the scattering volume may contribute to the spectral broadening, and be responsible for the observed angular dependence of the temperature values [9], Snyder *et al.* [10] have presented data that favor other broadening mechanisms for typical density variations in the jet. Since in our plasmas $kv_t/\nu_{ei}\sim 10-30$, collisional damping makes an important contribution in broadening the high-frequency part, $\omega\gtrsim kv_t$, of the density fluctuation spectrum. Our results, on the other hand, seem to confirm the fact that several mechanisms may be important in determining the spectral broadening: collisions, nonideality, and temperature gradients. Even if their relative contribution is unknown since these effects are lumped together, the memory function approach gives a very simple description of the resulting density fluctuation spectrum. Comparing Figs. 10 and 11, we see that the addition of helium in the jet has the effect that, on average, differences among the three models for the density fluctuations are less pronounced than for the pure argon plasma jet. This can be understood in terms of our analysis: adding helium in the plasma jet typically has the following effects: decrease in the electron density (due to the higher ionization potential than argon), increase in the electron temperature and increase in the thermal conductivity (see, e.g., Boulos *et al.* [33]). As a result, Γ decreases, (bringing the plasma closer to ideal), the electron-ion collision frequency also decreases, and the temperature gradients tend to be reduced.

VI. CONCLUSIONS

In this paper we have discussed a technique to analyze Thomson laser light-scattering data from weakly nonideal and collisional plasmas in the presence of temperature inho-

mogeneities. It is shown that the phenomenological description of the electron-density fluctuations based on the memory function formalism is more accurate than the standard random-phase approximation when plasma nonideality, collisionality, or inhomogeneity are significant in determining the dynamic structure of correlated systems. Indeed the preliminary results shown here seem to confirm that some of the problems reported in the past with Thomson scattering measurements of electron temperature and density can be avoided if the proposed approach is followed. In particular, electron temperature values obtained with this method are much less dependent on the scattering angle, with average values closer to the ones determined from spectroscopic measurements of line intensities. However, differences between the excitation temperatures obtained from spectroscopic measurements and the electron temperatures derived from Thomson scattering still exist.

ACKNOWLEDGMENT

This work was supported by the Engineering Research Program of the Office of Basic Energy Sciences of the U.S. Department of Energy under Grant No. FG02-85ER-13433.

[1] J.-P. Hansen and I.R. McDonald, *Theory of Simple Liquids* (Academic, London, 2000).
[2] G.A. Pavlov, *Transport Processes in Plasmas with Strong Coulomb Interaction* (Gordon and Breach, Amsterdam, 2000).
[3] E.E. Salpeter, Phys. Rev. **120**, 1528 (1960).
[4] D.E. Evans and J. Katzenstein, Rep. Prog. Phys. **32**, 207 (1969).
[5] S. Ichimaru, *Basic Principles of Plasma Physics* (Addison-Wesley, Reading, MA, 1973).
[6] J. Sheffield, *Plasma Scattering of Electromagnetic Radiation* (Academic, New York, 1975).
[7] S.C. Snyder, L.D. Reynolds, J.R. Fincke, G.D. Lassahn, J.D. Grandy, and T.E. Repetti, Phys. Rev. E **50**, 519 (1994).
[8] R.E. Bentley, J. Phys. D **30**, 2880 (1997).
[9] G. Gregori, J. Schein, P. Schwendinger, U. Kortshagen, J. Heberlein, and E. Pfender, Phys. Rev. E **59**, 2286 (1999).
[10] S.C. Snyder, D.M. Crawford, and J.R. Fincke, Phys. Rev. E **61**, 1920 (2000).
[11] S. Ichimaru, Rev. Mod. Phys. **54**, 1017 (1982).
[12] A.A. Valuev, A.S. Kaklyugin, and G.E. Norman, Sov. Phys. JETP **86**, 480 (1998).
[13] J.-P. Hansen and I.R. McDonald, Phys. Rev. A **23**, 2041 (1981).
[14] P.G. de Gennes, Physica (Amsterdam) **25**, 825 (1959).
[15] B. Brami and F. Joly, Physica A **139**, 306 (1986).
[16] J.-P. Hansen, in *Molecular Dynamics Simulation of Statistical Mechanical Systems*, edited by G. Ciccotti and W.G. Hoover, (North-Holland, Amsterdam, 1986), Vol. 97.
[17] D.D. Carley, Phys. Rev. **131**, 1406 (1963).
[18] S.G. Brush, H.L. Sahlin, and E. Teller, J. Chem. Phys. **45**, 2102 (1966).
[19] E.J. Linnebur and J.J. Duderstadt, Phys. Fluids **16**, 665 (1973).
[20] M. Baus and J.-P. Hansen, Phys. Rep. **59**, 1 (1980).
[21] R. Cauble and D.B. Boercker, Phys. Rev. A **28**, 944 (1983).
[22] P. Vieillefosse and J.-P. Hansen, Phys. Rev. A **12**, 1106 (1975).
[23] H.B. Singh, A. Sharma, and K.N. Pathak, Phys. Rev. A **19**, 899 (1979).
[24] J.-P. Hansen, I.R. McDonald, and E.L. Pollock, Phys. Rev. A **11**, 1025 (1975).
[25] M.C.M. van de Sanden, G.M. Janssen, J.M. de Regt, D.C. Schram, J.A.M. van der Mullen, and B. van der Sijde, Rev. Sci. Instrum. **63**, 3369 (1992).
[26] W.H. Press, S.A. Teukolsky, W.T. Vetterling, and B.P. Flannery, *Numerical Recipes* (Cambridge University Press, Cambridge, England, 1994).
[27] W. Rozmus, S.H. Glenzer, K.G. Estabrook, H.A. Baldis, and B.J. MacGowan, Astrophys. J. **127**, 459 (2000).
[28] C.S. Liu and V.K. Tripathi, *Interaction of Electromagnetic Waves with Electron Beams and Plasmas* (World Scientific, Singapore, 1994).
[29] A.V. Maksimov, K.N. Ovchinnikov, V.P. Silin, and S.A. Uryupin, Sov. Phys. JETP **86**, 710 (1998).
[30] D.B. Boercker, R.W. Lee, and F.J. Rogers, J. Phys. B **16**, 3279 (1983).
[31] W.L.T. Chen, J. Heberlein, and E. Pfender, Plasma Chem. Plasma Process. **14**, 317 (1994).
[32] H. Röhr, Z. Phys. **209**, 295 (1968).
[33] M. I. Boulos, P. Fauchais, and E. Pfender, *Thermal Plasmas: Fundamentals and Applications* (Plenum Press, New York, 1994), Vol. 1.